doi.org/10.15407/tpwj2017.09.04

FEATURES OF THE STRUCTURE OF PLASMA-ARC COATINGS PRODUCED AT APPLICATION OF FLUX-CORED WIRES WITH A STEEL SHEATH AND FILLER FROM B_4C AND ZrO_2 NANOPOWDER

G.M. GRIGORENKO, L.I. ADEEVA, A.Yu. TUNIK, V.N. KORZHIK and **L.M. KAPITANCHUK**
E.O. Paton Electric Welding Institute, NASU
11 Kazimir Malevich Str., 03150, Kiev, Ukraine. E-mail: office@paton.kiev.ua

Features of the structure of coatings made by high-speed plasma-arc spraying of wire with a steel sheath and B_4C powder filler with addition of nanosized ZrO_2 powder were studied. Coatings with low porosity (about 1 %), lamellar structure and high hardness were produced on a low-carbon steel substrate. Processes of interaction, running in plasma-arc spraying between the sheath, making up 90 wt.% of the wire, and the filler, were analyzed. Ferrite matrix of the coating is alloyed with boron and carbon, and contains an amorphous phase. It is strengthened by dispersed carbide, borocarbide and oxide particles. Addition of 0.5 % of ZrO_2 nanopowder promotes refinement of the coating structure with formation of dispersed borocarbides $Fe_3(B, C)$, $Fe(B, C)_2$, and oxides of iron FeO and boron B_3O_5. Coating microhardness reaches 6.86 GPa that is 4 times greater than that of the ferrite sheath. Coatings of this class can be applied as wear-resistant ones for protection of equipment from gas-abrasive wear in chemical engineering, in manufacturing parts of pumps, compressors and other items, as well as reconditioning worn parts. 22 Ref., 7 Tables, 7 Figures.

Keywords: *plasma-arc spaying, flux-cored wire, carbide filler, nanopowders, phase transformation, lamellar structure, dispersed strengthening of coatings, iron boro-carbide, microhardness*

Nowadays, high-speed electric arc spraying of wire materials in the flow of products of natural gas combustion with air is one of the progressive methods, which allows producing the highest quality coatings [1, 2]. Modern mechanical engineering makes ever higher requirements to coating wear resistance, which can be met only on the basis of new approaches. These are requirements of providing high density and strength of the coating, close to those of the compact material, minimum losses at spraying in the case of application of expensive materials and large volumes. Promising for solution of such problems is the process of plasma-arc spraying (PAS) with flux-cored wire at application of argon arc, blown by intensive concomitant air flow, increasing the plasma jet velocity [3–7]. At PAS of coatings, heating of wire material, its melting and formation of finely-dispersed sprayed particles occur both as a result of energy evolving in the arc anode spot, and closed on the wire, and due to energy applied to the wire at its transverse blowing by arc plasma flow. As a result, effectiveness of the process of wire melting rises essentially, compared to, for instance, traditional method of arc spraying [8]. Efficiency and stability of the process will be largely determined by conditions of heat exchange between the wire-anode and heat sources applied to it [3, 9]. Chemical and phase composition of flux-cored wire charge can be broadly varied, that opens up considerable possibilities for development of new coating systems, and, thus, for further widening the area of their practical application [10, 11]. Addition of nanosized additives to powder filler composition is one of the promising directions of improving the produced coating quality [12, 13].

The objective of this work is investigation of the structure, phase composition and properties of the composite coatings, produced by PAS from flux-cored wires with a steel sheath with fillers from B_4C and B_4C with addition of ZrO_2 (nanosized) powders. It is promising to use boron carbide as filler for flux-cored wires. Owing to its unique properties (high hardness (49.5 GPa, wear resistance, chemical resistance, etc.), it is becoming widely applied in modern engineering both in its pure form, and in the form of cermets [14]. Boron carbide interaction with the wire sheath is determined by chemical affinity of iron to boron and carbon. As is known , in Fe–B–C system the reaction of interaction at heating in shielding gas medium leads, primarily, to formation of stable iron borides FeB, Fe_2B, and then to formation of cementite Fe_3C. Carbon, contained in Fe–C melts, demonstrates high interphase activity, relative to B_4C with formation of boride and boron-carbide phases [15–17]. Fe–B system at rapid cooling (10^5–10^7 °C/s) is characterized by

Table 1. Characteristics of initial materials

Material	Particle size (grains), μm	Microhardness *HV* 0.25, GPa	Phase composition by XSPA data, wt.%
B_4C	40–100	29.96 ± 3.06	92.3 B_4C+7.7 C
ZrO_2	(2.6–7.3) 10^{-4}	–	92.2 $ZrO_{2(m)}$ + 7.8 $ZrO_{2(t)}$
St08kp	4–20	1.55 ± 0.7	100 α-Fe

formation of amorphous structures with high hardness of the order of 10 GPa. At PAS the processes of interaction run between the lower-melting steel sheath of the wire and refractory B_4C and ZrO_2 powder fillers. These processes lead to formation of new phases of a complex composition. At up to 10 wt.% B_4C, a fine-grain matrix structure forms, including dispersed borides, not forming any frame. Such materials are characterized by high strength (σ_t = 700 MPa) [18, 19]. Particles of nanosized refractory powder of ZrO_2 are added to the composition of flux-cored wire filler, in order to create additional crystallization centers at coating formation.

This work is a study of plasma-arc coatings from flux-cored wires, which were deposited on the base from low-carbon, low-alloyed steel with microhardness of 1.90 ± 0.2 GPa.

Investigation procedures and materials. A complex procedure was used in this work, including: metallography — Neophot-32 optical microscope with an attachment for digital photography; durometric analysis — LECO M-400 hardness meter at 0.249 and 0.496 N loads; X-ray structural phase analysis (XSPA) — DRON-UM1 diffractometer with CuK_α-monochromatic radiation. Electronic study of the structure and determination of its elementary composition by the method of X-ray spectral microanalysis (XSMA) were conducted in analytical system JAMP-9500F. JAMP-9500F system is fitted with energy-dispersive spectrometer OXFORD EDS INCA Energy 350 for analysis of elements from beryllium to uranium. Energy separating capacity is equal to $\Delta E/E$ = 0.005–0.6 %. This attachment allows determination of mass fraction (concentration) of chemical elements in the samples by the method of non-destructive energy-dispersive X-ray analysis. At application of energy-dispersive analysis, probe diameter is 1 μm, and at Auger-study it is 3 nm. The image of the structure was obtained in secondary electron mode (SEI) at U = 20 kV.

Reagents for chemical etching were used to reveal the structure of the studied objects. Structure of iron-based matrix was revealed in Nital reactive (4 % alcoholic solution of nitric acid, τ = 5–30 s, at t = 20 °C), that of boride component — using 10 % alcoholic solution of iodine (τ = 5–15 s, at t = 20 °C).

In 1.8 mm flux-cored wires a strip from low-carbon steel St08kp (rimmed) 0.3 mm thick with an overlap butt joint was used as the sheath. Steel structure consisted of equiaxed ferrite grains and thin pearlite interlayers along the grain boundaries.

Powders of boron carbide (100 % B_4C) and boron carbide with ZrO_2 additives (99.5 % B_4C + 0.5 % ZrO_2) were applied as wire fillers to study the influence of additives of zirconia nanopowder on formation of the structure and properties of composite coatings. Coefficient of wire filling was equal to about

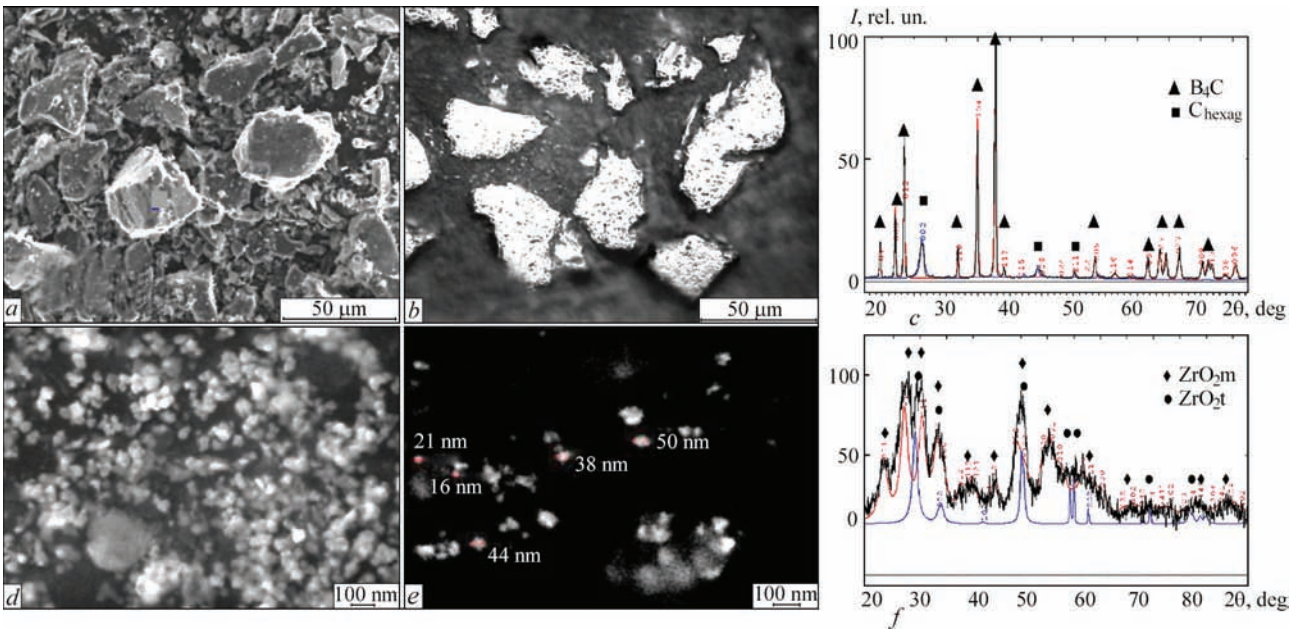

Figure 1. Morphology (*a*, *d*, *e*), microstructure (*b*) and roentgenograms (*c*, *f*) of powder filler particles: *a*–*c* — B_4C; *d*–*f* — ZrO_2

Table 2. Characteristics of PAS coatings produced from flux-cored wires

Filler composition, wt.%	*I*, A	Thickness, μm	Main phase components by XSPA data	Microhardness, GPa
100 B_4C	250	550	Fe_3B, α- Fe	6.76 ± 1.22
99.5 B_4C + 0.5 ZrO_2	240	300	Fe_3B, α-Fe	6.86 ± 2.10
Note. Porosity is 1.0 vol.%.				

9 wt.%. Characteristics of materials, making up the flux-cored wire, are given in Table 1.

B_4C powder, produced by ingot crushing, consists of particles of irregular fragmentary form of 40–100 μm size (Figure 1, *a*, *b*). Microhardness of powder particles is equal to 21.40–35.00 GPa. By the data of XSPA (Figure 1, *c*, Table 1) the main phase of the powder is B_4C with the following rhombic lattice parameters: a = 0.56078, c = 1.20897 nm and small amount of carbon with the following hexagonal lattice parameters: a = 0.24658, c = 0.67849 nm.

Morphological studies of nanopowder particles showed that the size of ZrO_2 particles does not exceed 100 nm (Figure 1, *d*, *e*). XSPA method was used to determine (Figure 1, *f*; Table 1), that zirconia nanopowder ZrO_2 consists of two modifications: monoclynic with lattice parameters: a = 0.51382, b = 0.51970, c = = 0.53078 nm and tetragonal with parameters of the lattice: a = 0.35997; c = 0.51692 nm.

Experimental. Coatings from flux-cored wires were produced by PAS method in PLAZER-30 unit in the following modes: I = 240–250 A; U = 60 V; L = 175 mm, Q_{air} = 110 l/min, Q_{Ar} = 7 l/min, wire feed rate — 7 m/min [20]. Coating characteristics are given in Table 2.

Coatings produced by PAS from wires with fillers are sound from metallographic viewpoint. They are thinly-lamellar, dense, have no cracks, and adhere well to the base. In the section of the coating with B_4C filler (Figure 2, *a*) dark inclusions of a spherical shape of 10–40 μm diameter and those of irregular shape of 80×100, 90×120 μm size are observed, as well as those in the form of lamellas of 15×110, 20×120 μm size (form factor of 7, 6). These inclusions are the initial boron carbide, which has not reacted with the steel sheath of the wire. Also observed are thin grey-coloured oxide fringes of 0.1–0.5 μm thickness along the lamella boundaries and small oxide particles of 1–10 μm diameter. After etching the section in Nital reagent it was found that the coating structure is predominantly lamellar with lamella size of approximately 20×70, 12×320 μm (form factor of 3–25). Lamellas of white colour and different shades of grey are observed. White lamellas and spherical particles of 10–30 μm diameter, have the highest microhardness of up to 12.5 GPa, and are an amorphous component of the coating. XSPA method confirmed the presence of amorphous phase in both the coatings — by recording a «Halo» in the roentgenograms in angular intervals of $39^\circ \le 2\theta \le 50^\circ$ and $79^\circ \le 2\theta \le 85^\circ$ (Figure 2, *b*, *d*) [21].

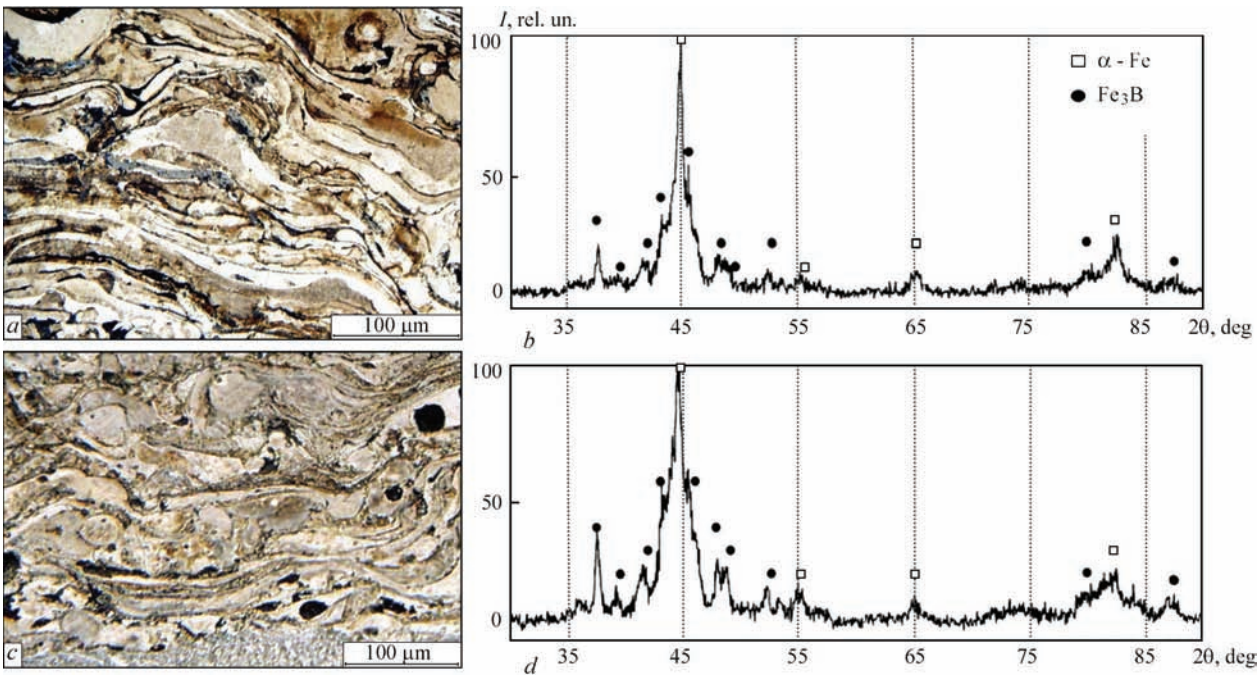

Figure 2. Microstructure (*a*, *c*) and roentgenograms (*b*, *d*) of plasma coatings produced from flux-cored wires with fillers of: *a*, *b* — B_4C; *c*, *d* — B_4C + ZrO_2

At high magnification it is found that grey lamellas consist of finely-dispersed round and platelike inclusions of borides and borocarbides in the iron-based matrix, i.e. they have a two-phase structure. The grey lamella microhardness is equal to 5.71 ± 1.22, and that of light-grey ones is 7.89 ± 1.35 GPa, that is attributed to their alloying.

In the coating produced by PAS from wire with $B_4C + ZrO_2$ filler, the structure also is predominantly lamellar with oxide interlayers along the lamella boundaries (Figure 2, *c*). Metal particles of a spherical shape of 15–100 μm diameter are rare. Oxide component is recorded in the form of individual particles of round and irregular shape, as well as interlayers along the boundaries of lamellas and round particles. The coating is characterized by different etchability of the structural components. After etching in Nital reagent, particles and lamellas of white, light-grey and grey colour are found. A structure with directional solidification or formation of an acicular-type structure, are recorded in thin lamellas. A cast dendritic structure is characteristic for thicker lamellas, and particularly, for round particles. Coatings are formed by rather large lamellas. Their maximum size reaches 500×30 μm, and the form factor of the lamellas is 5–17.

Studying the structure reveals white unetchable lamellas of amorphous type with high microhardness that is characteristic for Fe–B system, and is indicative of high rates of coating cooling. The quantity of such lamellas is about 15 vol.%, and their microhardness

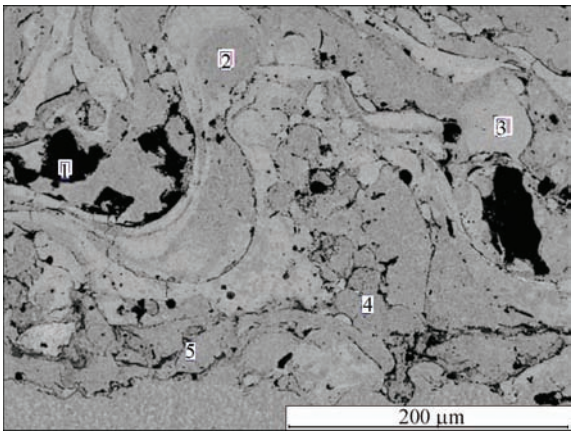

Figure 3. Microstructure of plasma coating produced from wire with $B_4C + ZrO_2$ filler (REM, BEI mode)

is in the range of 6.44–11.45 GPa. The initial boron carbide is recorded in the structure, which is present, mainly, in the form of globular dark-coloured particles of up to 50 μm size. After etching into the boride component, particles of iron boride of 0.5–1.0 μm size are observed in the structure. They are uniformly distributed across the entire coating thickness. Microhardness of such areas is equal to 5.49–12.83, and average microhardness of the coating is equal to 6.86 ± 2.10 GPa. This more than 4 times exceeds the microhardness of the steel sheath, which makes up about 90 wt.% of the wire. Addition of 0.5 % of ZrO_2 nanopowder to the composition of the wire filler only slightly increases the coating microhardness. By the data of XSPA and metallographic analysis, the main phases are: iron boride (Fe_3B), and α-Fe-based

Table 3. Composition of the studied coating areas (Figure 3)

Studied area	Element content, wt./at.%				
	Fe	B	C	O	Zr
1	4.02/0.82	72.56/76.95	22.99/1.95	0.38/0.27	0.03/0.00
2	96.52/84.74	2.35/10.64	1.13/4.62	0.00/0.00	0.00/0.00
3	95.91/82.48	2.80/2.43	1.21/4.83	0.08/0.25	0.00/0.00
4	97.67/89.67	1.38/6.54	0.71/3.01	0.24/0.78	0.00/0.00
5	73.5444.04	0.50/1.53	0.75/2.09	24.97/52.19	0.00/0.00
Note. Content of Mn ≤ 0.25 wt.%.					

Table 4. Composition of the studied coating areas (Figure 4)

Studied area	Element content, wt./at.%				
	Fe	B	C	O	Zr
1	96.33/84.24	2.37/10.72	1.12/4.54	0.14/0.43	0.00/0.00
	82.80	9.40	1.40	6.50	–
2	96.69/86.71	1.98/9.18	0.89/3.72	0.00/0.00	0.00/0.00
	85.3	7.20	0.70	6.80	–
3	98.46/93.68	0.26/1.28	0.90/4.00	0.27/0.89	0.00/0.00
4	97.91/93.05	0.64/3.13	0.61/2.70	0.15/0.50	0.18/0.10
5	6.04/1.29	68.24/75.28	23.11/22.95	0.21/0.15	2.24/0.29
	2.40	67.60	25.50	4.50	–
6	3.32/0.68	75.39/79.35	20.89/19.79	0.18/0.13	0.08/0.01
7	7.76/1.74	63.00/73.05	23.24/24.25	0.15/0.12	5.70/0.78
8	49.40	0.00	0.20	50.40	–
Note. Data of XSMA (not highlighted); Auger-spectrometry (highlighted by grey colour); content of Mn ≤ 0.48 wt.%.					

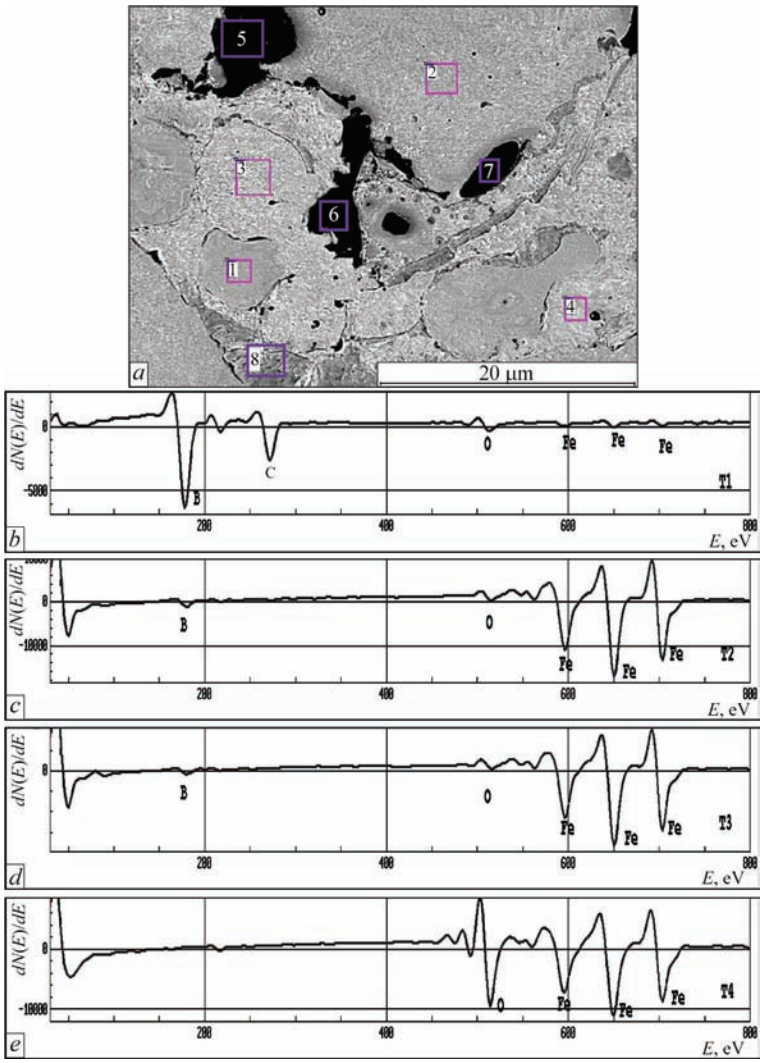

Figure 4. Microstructure (*a*) and Auger-spectrometry data (*b*–e) of areas 5, 1, 2, 8 of plasma coating produced from wire with B_4C + ZrO_2 filler, respectively

solid solution with larger parameter of BCC lattice, as well as boron carbide and iron oxide (FeO). Metastable Fe_3B phase was found in Fe–B system at rapid solidification at 10^{-3} °C/s. The phase has orthorhombic lattice with parameters a = 0.543; b = 0.666; c = 0.445 nm [22]. Parameters of this phase found in the coating, are somewhat different from the data of ASTM card file: a = 0.536; b = 0.668; c = 0.446 nm that is probably related to boride alloying by carbon, i.e. formation of borocementite.

Additional investigations were conducted using XSMA and Auger-spectroscopy methods, in order to study the influence of ZrO_2 nanopowder additives on formation of coating structure. Studied sections of the coating do not have a strict lamellar structure (Figure 3). Lamellas are bent, and their orientation is chaotic. In addition, rounded particles are found. Dark inclusions in the coating are boron carbide particles. Ferrite matrix, as a result of interaction with boron carbide at spraying, contains an increased quantity of boron and carbon. Coating areas, most doped with these elements, cannot be etched. They are white-coloured and smooth in optic photos. By the data of XSMA such particles and lamellas contain, wt.%: 2.1–3.6 B, and 1.1–1.8 C (Tables 3, 4: Figure 3, ar. 2, 3 and Figure 4, ar. 1). Deeper etched areas (light-grey lamellas in optic photos) contain 1.4–2.0 B and 0.7–0.8 C. These areas are more doped with boron, than with carbon (Tables 3, 4; Figure 3, ar. 4 and Figure 4, ar. 2). Studies of these areas performed in Auger-spectrometer, confirm the high concentration of boron and carbon in them (Table 4, Figure 4). Oxide lamella (Figure 4, ar. 8) is iron oxide FeO. The most heavily etched areas (grey-coloured lamellas in optic photos) contain wt.%: 0.3–0.6 B and 0.4–0.9 C (Table 4; Figure 4, ar. 3, 4).

Having studied element distribution in the characteristic radiation of Fe, B, O and C, we can conclude that the greatest amount of boron and carbon is contained in boron carbide areas. The wire sheath from carbon steel, the share of which in the coating is about 90 %, initially contains 0.08 wt.% C. By anal-

Table 5. Composition of studied areas of the coating (Figure 5)

Studied area	Element content, wt./at.%				
	Fe	B	C	O	Zr
Figure 5, *a*					
1	89.80/64.10	8.33/30.71	1.36/4.52	0.12/0.31	–
2	67.81/29.62	26.37/59.52	5.10/10.37	0.16/0.25	–
3	8.19/1.74	67.73/74.53	23.60/23.38	0.47/0.35	–
4	65.36/27.31	25.91/55.93	8.30/16.13	0.43/0.63	–
5	87.53/59.54	9.31/32.71	1.88/5.93	0.52/1.23	–
6	94.65/79.47	3.30/14.33	1.34/5.22	0.15/0.44	–
Figure 5, *b*					
1	16.87/4.19	55.23/70.81	20.35/23.48	0.35/0.30	6.13/0.93
2	92.38/70.91	5.83/23.11	1.54/5.50	0.07/0.19	0.00/0.00
3	98.36/93.57	0.45/2.21	0.81/3.60	0.00/0.00	0.08/0.04
4	57.28/21.87	27.68/54.59	12.84/22.79	0.17/0.23	1.70/0.40
5	90.13/64.42	7.94/29.31	1.85/6.16	0.00/0.00	0.00/0.00

Note. Content of Al, Si and Mn ≤ 0.3, 0.07 and 0.67 wt.%, respectively.

ysis results, all the lamellas in the coating have excess amount of boron and carbon. Enrichment of all the matrix components by these elements is the result of B_4C interaction with the wire sheath in spraying. Zr traces were found in matrix areas analyzed using XSMA method (Table 4; Figure 4, ar. 4). Recorded in the structure is the initial boron carbide, which is mainly present in the form of small-sized particles. At spraying, as a result of interaction with the plasma jet, boron carbide particles lose boron because of interaction with iron and boride formation. By the data of XSMA and Auger-spectrometry, boron carbide particles, remaining in the coating, correspond to the composition of $B_{2.5}$–B_4C (Tables 3–5; Figures 3–5). Zirconium in the amount of 2.2–5.7 wt.% was found in the most disintegrated boron carbide particles (Table 4). This is attributable to reaction of interaction between ZrO_2 and B_4C, which leads to zirconium recovery. A fringe with a changed structure 0.8–1.5 μm thick, enriched with B and C, is found around such particles (Table 5; Figure 5, *a*, ar. 1, 4–6 and Figure 5, *b*, ar. 2, 5). Such a fringe is absent around boron carbide of the initial composition — B_4C (Figure 4, ar. 6).

Figure 5, *a* and Table 5 give the structure and chemical composition of the matrix, located around partially disintegrated particle of boron carbide (B_3C). Nanosized particles of iron diboride — FeB_2, enriched with 5.1–8.3 wt.% C, are visible in the direct vicinity of the carbide to the depth of 0.1 μm (Figure 5, *a*, ar. 2, 4). Among the known iron borides, iron diboride features high hardness of 29–30 GPa. Beyond this zone, to the depth of 1.5 μm, the matrix structure is modified, becoming smooth. At 0.4–0.9 μm distance from boron carbide (Figure 5, *a*, ar. 5, 6), B and C content in the matrix decreases and is equal to 9.3–3.3 and 1.9–1.3 wt.%, respectively. The more intensive the carbide dissolution, the wider is the zone around it, enriched in these elements. Boron carbide fringe of $B_{2.5}C$ composition increased up to 2–3 μm (Table 5; Figure 5, *b*). It is alloyed with boron and carbon to a greater degree than is the coating matrix as a whole. In the ferritic matrix the average boron content is equal to approximately 1.5, and that of carbon is approximately 1.0 wt.%. At analysis of the composition of boron carbide in the matrix area adjacent to it, 6.1 and 1.7 wt.% Zr and an increased oxygen content were recorded (Table 5; Figure 5, *b*, ar. 1, 4). Nanosized particles of iron diboride formed in this area of the matrix, ZrO_2 nanoparticles participating in their formation.

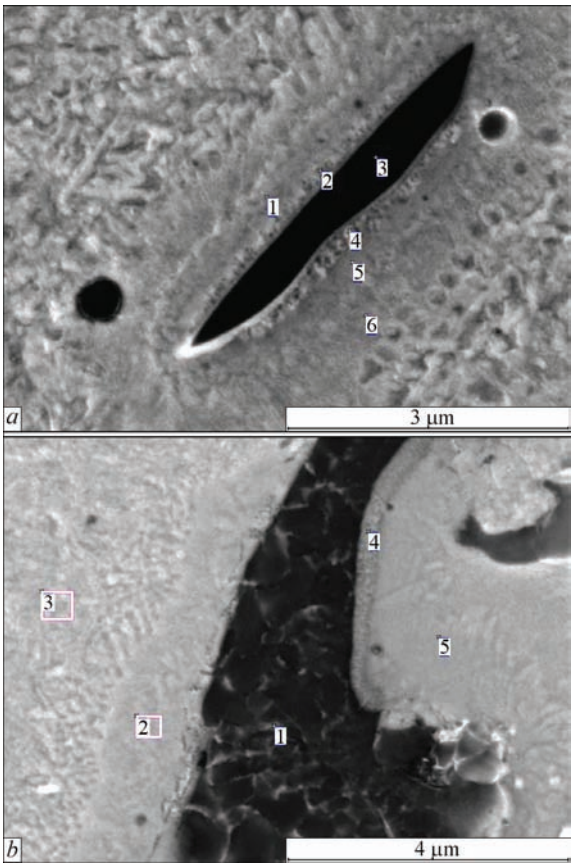

Figure 5. Matrix microstructure around B_4C inclusions (REM, BEI mode)

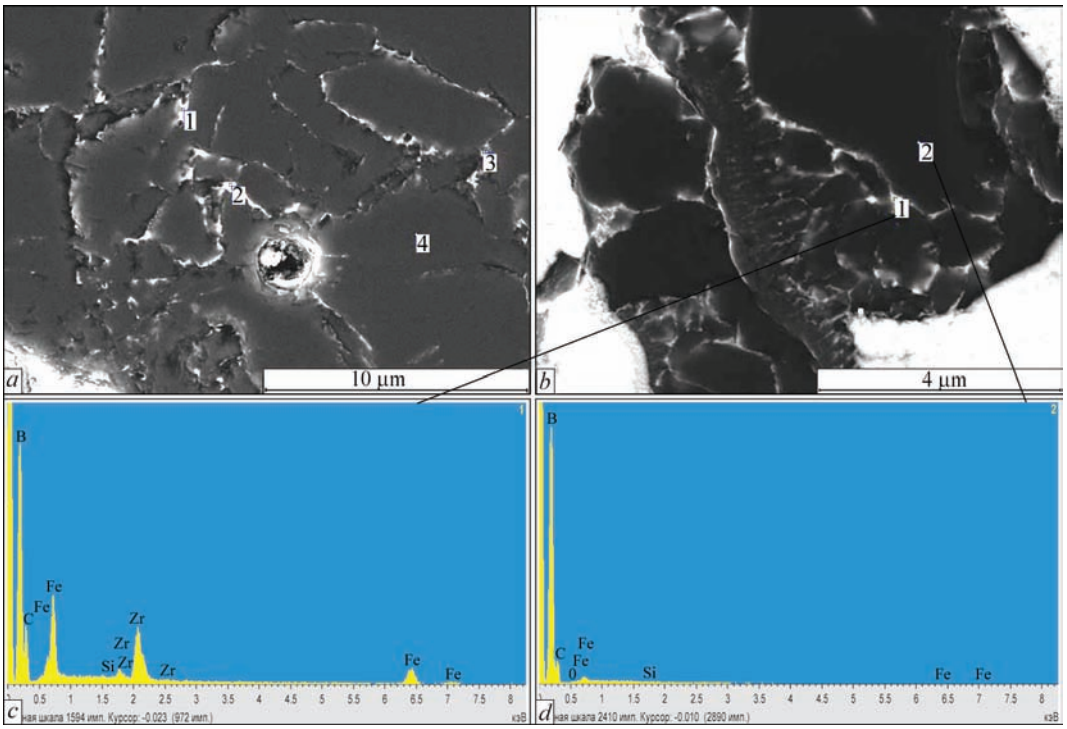

Figure 6. Microstructure (*a*, *b*) of boron carbide inclusions in the coating (REM, BEI mode) and spectra of areas 1 (*c*) and 2 (*d*)

When studying the structure of boron carbides in the coating, their grain structure is recorded (Figure 6). Segregations of the following elements were found along the boundaries of boron carbide grains, wt.%: 0.25–1.6 Zr; 22.0–52.0 Fe; 0.4–0.7 [O] (Table 6; Figure 6, *a*, ar. 1–4), compared to the grain bulk, where no enrichment with these elements was observed. This is clearly recorded in XSMA spectra, obtained from these areas (Figure 6, *b*, ar. 1, 2). These segregations are the result of interaction of powder filler components (ZrO_2 and B_4C) at spraying.

Chemical composition of nonmetallic components of the coating was determined by XSMA and Auger-spectrometry methods. The oxide component is

Table 6. Composition of studied coating areas (Figure 6)

Studied area	Element content, wt./at.%				
	Fe	B	C	O	Zr
Figure 6, *a*					
1	37.11/10.81	47.33/70.66	12.96/17.41	0.56/0.57	1.59/0.28
2	52.04/18.26	36.27/65.34	9.53/15.46	0.21/0.26	1.40/0.30
3	26.29/7.07	50.77/67.77	20.15/24.20	0.69/0.63	0.32/0.05
4	0.90/1.27	75.68/78.72	22.26/20.84	0.00/0.00	0.00/0.00
Figure 6, *b*					
1	21.86/0.25	52.15/71.71	16.55/20.49	0.39/0.36	0.25/1.38
2	1.63/0.07	74.67/77.66	23.37/21.87	0.15/0.11	0.07/0.01
Note. Content of Al, Si and Mn ≤ 0.17, 0.04 and 0.69 wt.%, respectively.					

Table 7. Composition of studied coating areas (Figure 7)

Studied area	Element content, wt./at.%					
	Fe	B	C	O	Mn	Zr
Figure 7, *a*						
1	78.53/45.56	11.43/34.25	0.92/2.48	8.63/17.48	0.21/0.12	0.28/0.10
2	65.41/33.74	12.74/33.94	0.28/0.68	15.73/28.31	4.29/2.25	0.76/0.24
3	32.75/11.02	19.28/33.52	0.75/1.17	45.67/53.66	0.86/0.29	0.29/0.06
4	95.90/83.70	1.92/8.66	1.35/5.48	0.54/1.64	0.00/0.00	0.00/0.00
Figure 7, *b*						
1	73.02/42.34	3.86/11.55	0.95/2.57	21.23/42.96	0.91/0.53	–
2	85.48/61.53	1.26/4.68	0.59/1.97	12.64/31.76	0.00/0.00	–
3	61.55/30.72	4.26/10.98	0.67/1.55	32.14/55.99	1.27/0.64	–
4	78.92/48.63	8.43/26.83	0.06/0.18	10.37/22.30	1.18/0.74	–

recorded in the form of fine oxide lamellas (5×18 μm, form factor of 3.5), individual particles of round or irregular shape of up to 10 μm size, as well as interlayers along the lamellas boundaries, predominantly 0.1–0.3 μm thick. As was noted above, small oxide lamellas in the coating correspond to FeO composition (Figure 4, Table 4). In fine globular inclusions of oxide type, of up to 1 μm size (Table 7, Figure 7, *a*, ar. 1, 2) the amount of boron exceeds that of oxygen, and they, essentially, are iron boro-oxide. Some of these inclusions are boron oxide, alloyed by iron (Table 7, Figure 7, *a*, ar. 3). Zirconium is often found in fine non-metallic inclusions in a small amount of 0.3–0.8 wt.%. It is obvious that at spraying ZrO_2 nanopowder interacts with the forming particles of iron boro-oxide and boron oxide. ZrO_2 particles in the coating matrix promote its fine-grain crystallization. As shown by investigations, the composition of oxide inclusions is non-uniform. So, globular iron oxide of 1.4 μm diameter at 0.13, 0.3 and 0.5 μm distance from the center contains 1.3; 3.9; and 4.3 boron, and 12.6; 21.0 and 32.0 wt.% oxygen, respectively (Table 7; Figure 7, *b*, ar. 1–3), i.e. the amount of these elements increases from the center to the edge of FeO nonmetallic inclusion, alloyed with boron. Having analyzed many oxide inclusions, we can conclude that their composition is complex: FeO iron oxide is alloyed with boron, and boron oxide contains iron. Here, dispersed particles of boron oxide are more common, than those of iron oxide. They have a globular shape of the diameter from 100 nm up to several μm, and are particles strengthening the matrix.

Conducted comprehensive studies allowed determination of the following composition of the coatings: iron boro-carbides ($Fe_3(B,C)$; $Fe(B,C)_2$); α-Fe with increased lattice parameters, as a result of alloying by boron and carbon; amorphous phase; boron carbide of variable composition ($B_{2.5}C$–B_4C); Fe boro-oxide; Fe and B oxides.

In conclusion it can be noted that owing to broad variation of filler composition, flux-cored wires are a promising material for PAS of protective wear-resistant coatings. Defect-free coatings with lamellar structure and low porosity (about 1 %), are produced from flux-cored wires with fillers of B_4C and B_4C with addition of nanosized ZrO_2 powder. A dispersion-strengthened ferrite matrix of the coating forms as a result of interaction with the wire ferrite sheath. High hardness of the coatings is due to the following main structural factors:

- alloying of α-Fe based matrix by boron and carbon, owing to considerable dissociation of B_4C at spraying, and, as a result, formation of amorphous structures;

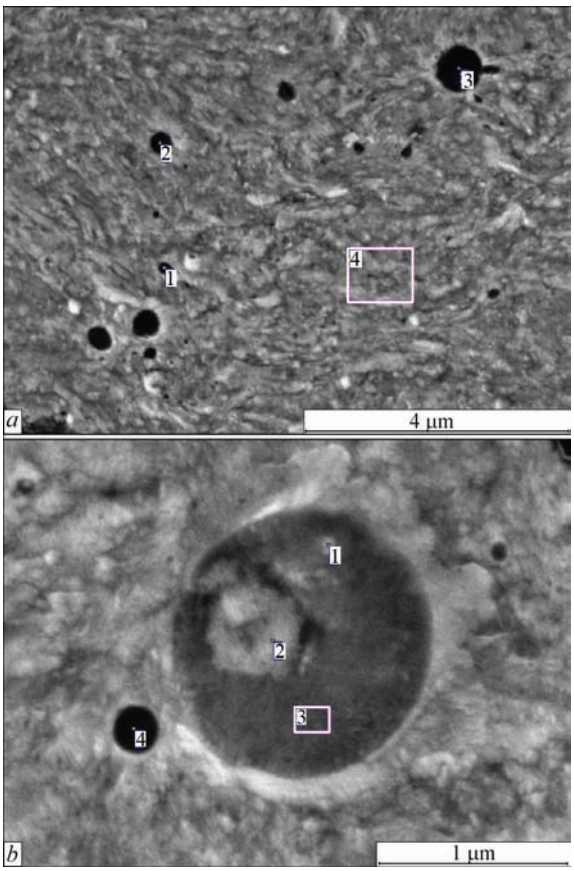

Figure 7. Microstructure of nonmetallic inclusions in the coating (REM, BEI mode)

- strengthening of coating matrix by uniformly distributed dispersed particles of $Fe_3(B_2C)$, $Fe(B,C)_2$ iron boro-carbides, iron boro-oxide and iron and boron oxides;
- strengthening by small, non-decomposed particles of boron carbide of a variable composition of B_4C–$B_{2.5}C$.

During spraying, ZrO_2 nanopowder additive reacts with B_4C, enriching its boundaries, and participates in formation of nanosized particles of iron diboride, dispersed oxides of iron (FeO) and boron (B_3O_5). Addition of ZrO_2 powder promotes refinement of the lamella structure, here coating microhardness is equal to 6.86 + 2.1 GPa, that is 4 times higher than that of the ferrite wire sheath.

Thus, PAS of the wire with steel sheath and powder filler of B_4C and $B_4C + 0.5ZrO_2$ resulted in producing a coating with uniform distribution of dispersed strengthening particles in the ferrite matrix. Coatings of this class can be applied as wear-resistant ones for protection from gas-abrasive wear of equipment in chemical engineering, in manufacture of parts of pumps, compressors and other products, as well as reconditioning worn parts.

1. Khromov, V.N., Vertsov, V.G., Korovin, A.Ya. et al. (2001) From subsonic to supersonic spraying of coatings in resto-

ration and strengthening of machine parts (Review). *Svarochn Proizvodstvo*, **2**, 39–47.
2. Kharlamov, Yu.A. (2000) Thermal spraying of coatings and ecological compatibility of production, service and repair of machines. *Tyazholoe Mashinostroenie*, **2**, 10–13.
3. Wielage, B., Rupprecht, C., Pokhmurska, H. (2011) Peculiarities of thermal spraying of coatings using flux-cored wire (Review). *The Paton Welding J*., **10**, 21–25.
4. Kharlamov, M.Yu., Krivtsun, I.V., Korzhik, V.N. et al. (2007) Mathematical model of arc plasma generated by plasmatron with anode wire. *Ibid*., **12**, 9–14.
5. Kharlamov, M.Yu., Krivtsun, I.V., Korzhik, V.N. et al. (2011) Heating and melting of anode wire in plasma arc spraying. *Ibid*., **5**, 2–7.
6. Wielage, B., Rupprecht, C., Bruhl, M. et al. (2008) Thermisches Spritzen — Potentiale, Entwicklungen, Maerkte. *Thermal Spray Bulletin*, **1**, DVS-Verlag, 30–36.
7. Petrov, S.V., Karp, I.N. (1993) *Plasma air-gas spraying*. Kiev: Naukova Dumka.
8. Kudinov, V.V., Bobrov, G.V. (1992) *Spraying deposition of coatings. Theory, technology and equipment*. Moscow: Metallurgiya.
9. Kharlamov, M.Yu., Krivtsun, I.V., Korzhik, V.N. et al. (2011) Formation of liquid metal film at the tip of wire-anode in plasma-arc spraying. *The Paton Welding J*., **12**, 2–6.
10. Borisov, Yu.S., Koziakov, I.A., Korzhik, V.N. (1996) Structure and properties of thermal coatings produced using flux-cored wires of Fe–Cr–B, Fe–Cr–B–C system. *Avtomatich. Svarka*, **5**, 21–24.
11. Pokhmursky, V.I., Student, M.M., Gvozdetsky, V.M. et al. (2011) Flux-cored wires of FMI series for coating deposition by electric arc spraying (Review). *Ibid*., **9**, 44–48.
12. Korotaev, A.D., Borisov, D.P., Moshkov, V.Yu. et al. (2005) Nanostructured and nanocomposite superhard coatings. *Phys. Mesomech*., 8(**5–6**), 93–104.
13. Vityaz, P.A., Ilyushchenko, A.F., Khejfets, M.L. (2011) *Technologies of structural nanostructured materials and coatings*. Ed. by P.A. Vityaz. Minsk: Belarus. Navuka.
14. Makarenko, G.N., Marrej, E.V. (1975) *Hard materials based on boron carbide. High-temperature carbides*. Kiev: Naukova Dumka, 133–136.
15. Panasyuk, A.D., Fomenko, V.S., Glebova, G.G. (1986) *Resistance of nonmetallic materials in melts*: Refer. Book. Kiev: Naukova Dumka.
16. Serebryakova, V.I., Neronov, V.A., Peshev, P.D. (1991) *High-temperature borides*. Moscow: Metallurgiya.
17. Grigorenko, G.M., Borisova, A.L., Borisov, Yu.S. et al. (2003) Investigation of interphase interaction of ferrotitanium with boron carbide in powder mixtures for thermal coating deposition. *Sovremennaya Elektrometallurgiya*, **1**, 28–31.
18. Tkachenko, V.F., Kogan, Yu.I. (1978) Peculiarities of structure and mechanical properties of sintered materials Fe–B_4C. *Poroshk. Metallurgiya*, **5**, 69–71.
19. Nevar, N.F., Fasevich, Yu.N., Senkov, V.M., Pavlovich, G.V. (2005) Boron-containing alloy, its characteristics and industrial application. *Litiyo i Metallurgiya*, **2–2**, 174–178.
20. Korzhik, V.N., Korob, M.F. (2012) Mechanized line PLAZER 30PL-W for plasma-arc wire spraying of coatings. *Svarshchik*, 86(**4**), 13–16.
21. Grigorenko, G.M., Korzhik, V.N., Adeeva, L.I. et al. (2016) Specifics of metallurgical processes in plasma-arc spraying of coatings produced from flux-cored wire with steel sheath and fillers B_4C and $B_4C + ZrO_2$. Visnyk PDTU. *Ser. Tekhnichni Nauky*, **32**, 125–138.
22. Chien, C.L., Musser, D., Gyorgy, E.M. et al. (1979) Magnetic properties of amorphous Fe_xB_{100-x}($72 \le x \le 86$) and crystalline Fe_3B. *Phys. Rev*. (Condens. Matter), 20(**1**), 283–295.

Received 07.04.2017